NIH-PA Author Manuscript

Technology Preview: X-Ray Fused With Magnetic Resonance During Invasive Cardiovascular Procedures

Luis F. Gutiérrez, PhD[1,2], **Ranil de Silva, MRCPPhD**[3], **Cengizhan Ozturk, MDPhD**[3,4], **Merdim Sonmez, MSc**[3,4], **Annette M. Stine, RN**[3], **Amish N. Raval, MD**[3], **Venkatesh K. Raman, MD**[3], **Vandana Sachdev, MD**[3], **Ronnier J. Aviles, MD**[3], **Myron A. Waclawiw, PhD**[5], **Elliot R. McVeigh, PhD**[1,2], and **Robert J. Lederman, MD**[3,*]

[1] *Laboratory of Cardiac Energetics, National Heart, Lung and Blood Institute, National Institutes of Health, Bethesda, Maryland* [2] *Department of Biomedical Engineering, Johns Hopkins University School of Medicine, Baltimore, Maryland* [3] *Cardiovascular Branch, National Heart, Lung and Blood Institute, National Institutes of Health, Bethesda, Maryland* [4] *Biomedical Engineering Institute, Bogazici University, Istanbul, Turkey* [5] *Division of Intramural Research and Office of Biostatistics Research, National Heart, Lung and Blood Institute, National Institutes of Health, Bethesda, Maryland*

Abstract

Background—We have developed and validated a system for real-time X-ray fused with magnetic resonance imaging, MRI (XFM), to guide catheter procedures with high spatial precision. Our implementation overlays roadmaps—MRI-derived soft-tissue features of interest—onto conventional X-ray fluoroscopy. We report our initial clinical experience applying XFM, using external fiducial markers, electrocardiogram (ECG)-gating, and automated real-time correction for gantry and table movement.

Methods—This prospective case series for technical development was approved by the NHLBI Institutional Review Board and included 19 subjects. Multimodality external fiducial markers were affixed to patients' skin before MRI, which included contrast-enhanced, 3D T1-weighted, or breath-held and ECG-gated 2D steady state free precession imaging at 1.5T. MRI-derived roadmaps were manually segmented while patients were transferred to a calibrated X-ray fluoroscopy system. Image spaces were registered using the fiducial markers and thereafter permitted unrestricted gantry rotation, table panning, and magnification changes. Static and ECG-gated MRI data were transformed from 3D to 2D to correspond with gantry and table position and combined with live X-ray images.

Results—Clinical procedures included graft coronary arteriography, right ventricular free-wall biopsy, and iliac and femoral artery recanalization and stenting. MRI roadmaps improved operator confidence, and in the biopsy cases, outperformed the best available alternative imaging modality. Registration errors were increased when external fiducial markers were affixed to more mobile skin positions, such as over the abdomen.

Conclusion—XFM using external fiducial markers is feasible during X-ray guided catheter treatments. Multimodality image fusion may prove a useful adjunct to invasive cardiovascular procedures.

*Correspondence to: Robert J. Lederman, Cardiovascular Branch, Building 10 Room 2C713, Bethesda, MD 20892-1538. E-mail: E-mail: ledermar@nhlbi.nih.gov.

Keywords

catheterization; magnetic resonance imaging; stereotactic surgery; image guided intervention; myocardial biopsy; chronic total occlusion

INTRODUCTION

Roadmapping refers to superposition of prior images with "live" or real-time images during invasive procedures. The most widely used form, digital subtraction angiography, subtracts the corresponding pixels in a recent radiocontrast angiogram from superposed live X-Ray fluoroscopy [1]. Roadmaps derived from disparate imaging modalities can be combined in several ways, ranging from computed tomography (CT) [2,3] or MRI-derived [4,5] myocardial images overlaid onto electro-anatomic maps, or magnetic resonance images combined with live "heads-up" optical surgical headsets [6].

The process of combining or "fusing" different imaging modalities requires registration of imaging data that exist in different image "spaces" depending on the acquisition modality. Volumetric or tomographic images acquired using MRI or CT need to be transformed before combining with 2D projections acquired using X-ray fluoroscopy. Approaches to image registration include (a) assuming that a patient is immobilized on a table that is moved and tracked between imaging modalities [7]; (b) attaching common reference points (known as fiducial markers) to the surface of the patient, and using the correspondence of those fiducial markers to warp the rest of the images until they overlap [8]; (c) using intrisinsic fiducial markers, such as bones or vessel bifurcations [9]; (d) using automated or manual manipulation of the image similarity to make them correspond [10]. Here, we test the second technique, which is attractive because it is amenable to real-time implementation, simple, robust, not reliant on multiple radio-contrast runs, and adjustable for patient movement.

Cardiovascular MRI can depict myocardial contractile function, perfusion, and viability; vessel anatomy by angiography; and blood flow and many other soft-tissue features. Real-time MRI has successfully guided interventional cardiovascular procedures in animal models, but requires specially designed catheter devices not yet available for human use. We have developed an intermediate approach to guide conventional fluoroscopic cardiovascular procedures by fusing 3D roadmaps derived from MRI onto the live 2D X-ray fluoroscopy images [11,12]. Our system provides some of the advanced functionality of interventional MRI using any conventional X-ray fluoroscopy system. In this pilot experience, we hypothesize that XFM provides enhanced target tissue visualization and increases the operator subjective ease-of-use.

METHODS

Human Subjects

The clinical protocol (NCT00064896) was approved by the NHLBI Institutional Review Board. Consecutive patients undergoing invasive procedures were invited to participate. All subjects consented to participate in writing and were investigated and treated at the NIH Clinical Center in Bethesda, MD.

Baseline MRI

MRI was performed at 1.5 T (Sonata, Siemens) using an eight channel phased array surface coil (Nova Medical). Gadopentate dimeglumine (*Magnevist*, Berlex) 0.2 mmol/kg was administered for contrast-enhanced examinations.

Cardiac regions of interest were contoured from multiple, breath-held, electrocardiogram (ECG)-gated cine steady-state free precession (SSFP) MRI using the following typical parameters: TR/TE (time to echo), 3.6/1.8 ms; flip angle, 65°; FOV, 300 mm × 244 mm; matrix, 256 × 127 pixels; slice thickness, 8 mm; bandwidth, 1085 Hz/pixel.

Arterial adventitial and luminal contours were derived from 3D contrast-enhanced MRA (typical parameters: TR/TE, 2.3/0.9 ms; flip angle, 25°; FOV, 512 × 314 × 122 mm matrix, 256 × 156 × 54; bandwidth 815 Hz/pixel), from 3D breath-held T1-weighted MRI (typical parameters: TR/TE, 6.2/2.3; flip angle, 12°; FOV 400 × 325 × 220 mm matrix 256 × 156 × 64; bandwidth, 200 Hz/pixel), and/or a high resolution reduced field of view (FOV) technique [13].

External fiducial markers were located using 3D T_1-weighted gradient echo (T_1W-GRE) using the following typical parameters: TR/TE, 2.37/1.18 ms; flip angle, 17°; FOV, 400 × 300 × 230 mm^3; matrix, 256 × 192 × 61 voxels; bandwidth, 1300 Hz/pixel. MRI gradient warping distortion was corrected at the scanner console [14]. Images were transferred to a commercial workstation for manual segmentation of regions of interest and external fiducial markers and then transferred to the XFM workstation within ~15 min.

XFM Registration Techniques

Figure 1 describes the workflow during XFM procedures. Custom dual modality X-Ray and MRI conspicuous fiducial markers (Beekley) contained 5 mM gadopentate dimeglumine and iodinated radiocontrast (iodixanol 320 mg I/mL, *Visipaque*, GE Medical). About 16 ± 3.0 markers were affixed using adhesive dressing to the skin surrounding the target anatomy immediately before baseline MRI. We attempted to distribute markers evenly around the target anatomy, including anterior, lateral, and posterior positions. Afterward, patients were transferred immediately for X-ray (Axiom Artis FC, Siemens, an image-intensifier system) using a mechanized transport table (Miyabi, Siemens). Because the live clinical X-ray fluoroscopy imaging chain is not accessible to end users, we captured the video output of the fluoroscopy system (downsampled to 512 × 512 pixels) using a video frame grabber (Accustream 170, Foresight Imaging) housed in an external computer. A capture interface was developed using Foresight's Visual C++ software development kit to import live data into MATLAB (Mathworks) at 8 frames/sec. Fusion images were displayed alongside live X-ray images.

Single- or multiphase images were registered using external fiducial markers and custom multimodality image processing fusion software developed in MAT-LAB. Briefly, fiducial marker locations in the X-ray and MR images were identified to provide corresponding points under X-ray and MRI coordinate systems. For registration, 3D fiducial marker locations on MRI were transformed to X-ray-like projections. The distance between matching fiducial marker locations was then minimized using a nonlinear least squares optimization, which iteratively fitted three variables defining a rotational matrix and three variables defining a translational vector to find the best rigid body transformation. The X-ray image intensifier also contributed distortions (pincushion distortion inherent in image-intensifier systems, sigmoidal distortion due to earth and MRI magnetic field effects, and geometric distortion due to nonuniform gantry sagging at different positions). These were corrected using empirical 2D fifth-order polynomials [11] acquired during a separate one-time calibration. This calibration process generated a lookup table for a range of gantry positions to best estimate the distortions at any specific position. In vitro phantom tests showed that the XFM representations of blood vessels were within 1 mm of the true position under X-ray [11]. In animal tests of catheter-based myocardial injection, we reported a target registration error of 3.2 ± 2.6 mm [12].

At the beginning of each clinical XFM procedure, three single-frame X-ray images were acquired of the fiducial markers at end expiration using maximum FOV at different gantry positions, typically spanning ~90° of obliquity, to register their coordinate positions within MRI and X-ray. Centers of fiducial markers were identified manually. The custom XFM software package continuously obtained gantry position, source-to-image distance, magnification settings, table height, and table (X–Y panning) position from the X-ray system and corrected the registration accordingly. If the patient motion was recognized or the registration accuracy was degraded, this short procedure could be repeated.

MRI information was represented as smoothed surfaces derived from B-spline tensors fitted to the manually drawn contours. These surfaces were registered with the X-ray coordinate system using the rigid body transformation computed above and then fused with live X-ray images displayed at eight frames per second on a separate live display.

ECG-Gated XFM

XFM could be performed using retrospective gating. During MRI, each frame corresponding to a phase in the cardiac cycle is tagged to indicate the time after the origin of the electrocardiographic QRS complex. During XFM, gating information (the time from the QRS) was measured continuously using a custom Labview (National Instruments) program controlling an analog to digital ECG acquisition system housed in the fusion computer. The image corresponding to the appropriate phase of the cardiac cycle was chosen from available MRI frames and displayed to the operator.

Measurement of Error and Data Analysis

Registration error was calculated from vessel center-lines (angiograms or adventitial contours in peripheral artery disease cases) and endocardial contour (ventriculograms in myocardial cases) during radiocontrast angiography. For each point along the MRI region of interest, the Euclidean distance was measured to the closest corresponding point on the X-ray image. Error is reported as root-mean square (RMS) of these 2D distances or presented as mean ± standard error of means for RMS error when subjects were combined. This measurement ignores the projection error, which is appropriate in instances such as XFM where 3D MRI data are represented in relation to 2D X-ray data.

Correlation is calculated as a Pearson moment coefficient. Continuous parameters are presented as mean ± standard deviation.

RESULTS

Subjects

Twenty procedures were conducted in 19 subjects having a median age of 66 (range 23–82). Eight were femoropopliteal revascularization procedures (six recanalization for occlusion), six were iliac procedures (three recanalization for occlusion), and six were diagnostic cardiac procedures (two including coronary grafts, one for native coronary arteries only, one pericardiocentesis, and two myocardial mass).

Case Example: Intracardiac Mass

In the first human test of the system, a 23-year-old man was referred for biopsy of a mass in the right ventricular free wall. A transvenous 7Fr bioptome (BIPAL, Cordis) was guided by fluoroscopy and intra-cardiac echocardiography using a 64-element phased-array 10 MHz 10Fr probe (Acunav, Acuson). Adjunctive XFM guidance was tested using 16 external fiducial markers, and overlaying manually defined regions of interest including separate endocardial borders of the right ventricle and of the mass. The source MR images used breath-held, ECG-

gated, segmented SSFP with 4 mm slices. The position of the bioptome was confirmed under fluoroscopic, intracardiac echo, and XFM guidance before each deployment of the bioptome jaws (Fig. 2).

Six specimens were obtained without complication. Histopathologic analysis revealed normal myocardium in each specimen, whereas excised pulmonary masses revealed inflammatory myofibroblastic tumor.

The 3D position of the bioptome was triangulated using XFM and two different X-ray gantry positions (Fig. 3A and 3B). This revealed discontinuity between the tip of the bioptome and the right ventricular mass. Retrospective analysis of the source MRI revealed a papillary muscle directly posterior to the right ventricular mass (Fig. 3E and 3F). Integrating this region of interest into the XFM clearly indicates that the biopsy specimens were obtained from the papillary muscle rather than from the tumor (Fig. 3G–3J).

In another subject requiring biopsy in the high inter-atrial septum, XFM was performed in addition to the conventional intracardiac and transesophageal echocardiography. XFM helped to avoid inadvertent atrial free wall and aortic biopsy (data not shown).

Case Example: Roadmaps From Contrast-Enhanced MR Angiograms

XFM using roadmaps from MR angiography provides a simple test of correspondence. Clinically, this can reduce exposure to iodinated radiocontrast and possibly ionizing radiation. Figure 4 demonstrates a roadmap derived from 3D contrast-enhanced magnetic resonance angiography under XFM during conventional iliac angiography. Unlike conventional radiocontrast roadmapping, these roadmaps remain valid even as X-ray angulation was altered and even after table panning. In this case, the registration error was 1.6 mm RMS.

Case Examples: Iliac Artery Revascularization and Registration Error

However, XFM did not provide consistently satisfactory roadmaps during iliac artery recanalization and angioplasty procedures. Figure 5 demonstrates two procedures during which registration was inadequate to guide catheter-based treatment. Figure 5A shows mis-registered lumen contours from MR angiography. Figure 5B shows misregistered adventitial contours from breath-held MRI in another patient. The overall mean registration error was 3.5 ± 1.9 mm RMS and probably was exacerbated by the displacement of fiducial markers affixed to abdominal skin. Registration error did not correlate with body mass index ($r^2 = 0.11$).

Registration was similarly unsatisfactory (noncorrespondence of the parietal pericardial contour) during pericardiocentesis, in which MRI was performed in a supine position but the invasive procedure was performed with the torso elevated by 35°. Repositioning the patient presumably displaced skin-based fiducial markers.

Case Example: Femoral Artery Recanalization

XFM was subjectively useful in guidewire recanalization of occluded superficial femoral arteries. Regions of interest, depicting the adventitial borders of the target artery, were extracted from T1-weighted (lumen-independent) spin-echo MRI studies. The XFM images assured guidewire trajectories remained within these adventitial confines and avoided, for example, geniculate and other collateral branches. This XFM implementation automatically corrects for X-ray tube and table position and is able to portray target artery contours even when a long occlusion spanned multiple X-ray fields of view. In five cases, in which XFM appeared qualitatively acceptable at the beginning of the procedure, the mean registration error was 2.3 ± 1.1 mm RMS. Figure 6 illustrates one patient in whom XFM assisted in the recanalization and stenting procedure. In this case, the registration error was 1.4 mm RMS.

Case Example: Coronary Arteriography, Ventriculography, and ECG-Gated XFM

XFM coregistration of MRI and X-ray fluoroscopy was tested in this patient undergoing transfemoral left ventriculography and selective injections of coronary artery bypass grafts. Endocardial and epicardial contours of the left ventricle were obtained at multiple phases of the cardiac cycle. These contours were synchronized with the real-time ECG during radiocontrast angiography as shown in Figure 7 and video supplements. The MRI-derived endocardial border corresponded qualitatively with the radiocontrast ventriculogram, although the registration error was 5.2 mm RMS. During selective arteriography, for example of a right internal mammary to left anterior descending coronary artery bypass graft, MRI-derived regions of interest were appropriately represented dynamically during extensive table panning across multiple fields of view.

In another representative patient, regions of interest such as myocardial infarction are displayed in context with the radiocontrast coronary arteriograms (data not shown).

The superposition of MRI regions of interest during table panning, even when X-ray fluoroscopy was not in use, enabled radiation-free positioning of the patient and X-ray gantry for subsequent acquisitions.

DISCUSSION

In this study, we describe our first clinical experience using a system to superimpose or "roadmap" findings from MRI examinations onto live X-ray during invasive cardiovascular procedures. The images are made to correspond based on the fiducial markers affixed to the skin during both examinations. The system maintains image correspondence throughout the cardiac cycle and even while the X-ray gantry and patient table are repositioned. Fusion images helped to overcome the individual limitations of each imaging modality. This approach, using fiducial markers, affixed to the patient could compensate for shifts in patient position on the table. XFM, using external fiducial markers, outperformed the best available alternative modality in one example of myocardial free wall biopsy, but suffered registration errors when the markers were placed on the mobile skin, especially over the abdominal wall. We provide a range of clinical examples illustrating the potential utility of XFM during invasive cardiovascular procedures.

Limitations of Roadmapping

Roadmapping using prior images can be valuable to guide catheter positioning, especially when the target tissue cannot be well visualized (e.g., occluded peripheral arteries, and masses), or when repeated contrast or radiation exposure is undesirable. However, roadmapping relies on prior information, which can become outdated. Rigid wires or catheter devices may distort vessel conformation (e.g., vessel straightening) and target tissues may change during the procedure (e.g., in intramural hematoma, rupture, or dissection). In the heart, volume and loading alterations may cause significant geometric variation between current and roadmapped historical representations of chamber size and position, especially if there is significant time disparity. Finally, uncorrected periodic and nonperiodic respiratory (speech, sighs, and deep breaths) and nonperiodic cardiac motion (irregular rhythm) also can contribute to the registration error [15–18]. Coordinating images during voluntary or controlled end expiration may reduce this error. The magnitude of these motion errors probably exceed tolerances permissible in coronary artery interventional procedures [19], but may prove acceptable for the structural heart disease and other endovascular procedures.

3D roadmaps may provide some of the functionality of biplane fluoroscopy systems using monoplane fluoroscopy systems. 3D roadmapping may also have value in selecting optimal views of complex or tortuous vascular bifurcations [20].

Limitations of External Fiducial Marker Techniques

Our system fuses images using a rigid body transformation to register rotated and translated roadmaps. It does not correct for nonrigid deformation like some image-based methods [21]. A common disadvantage of image-based methods is their comparatively long computation times. However, the two methods might be combined, for example, by first using rigid fiducial-based rigid body registration followed by nonrigid image-based registration for improved performance.

Our MRI-derived roadmaps were acquired during the same session as the invasive X-ray procedure. External fiducial marker beads remained in place during both component examinations, and the intermodality transfer table minimized patient movement. Transferring between nonadjacent MRI and X-ray labs, or removing and reapplying fiducial marker beads in separate sessions, could be expected to generate more error. Using previously acquired MR images (without fiducial markers) for XFM would not be possible in our system, without performing a second MRI to register the two MR acquisitions. We hope to develop this in the future.

We observed that external fiducial markers affixed to the skin of patients in this study performed less well than those affixed to the skin of juvenile animals during development [12]. The additional error presumably reflects gravitational shifts of the fiducial markers on loose abdominal skin of older and more obese human subjects, combined with variable respiratory motion. Nevertheless, there was no correlation between body mass index and registration error. Other techniques, such as affixing markers only over bony landmarks, or employing tight vests that incorporate markers, might reduce these shift errors. Retrospective respiratory gating also might improve registration. External markers may obscure imaging targets and add extraneous "visual flak" to images.

How to Measure Benefit?

It remains challenging to prove the benefit of incremental technical developments for image-guided intervention. Measures can include time savings or radiation exposure, success rate, or avoiding surgical alternatives. By comparison, the benefit of intravascular ultrasound during percutaneous coronary artery intervention has been inconsistent when tested in large clinical trials, even though it is widely considered a valuable or even essential element of coronary intervention by many operators [22]. In this small series, XFM improved subjective operator ease-of-use and confidence, although we provide no utility measures.

Future Steps

Additional useful functionality might include automatic identification, registration, and tracking of external fiducial markers, automatic segmentation especially of large ECG-gated time series to improve the clinical workflow of ECG-gated XFM, and automatic compensation for respiratory motion. Custom tight-fitting garments with embedded fiducial markers might constrain undesirable shifting of the markers and help automate marker registration. More complex but useful would be registration based on intrinsic fiducial markers, such as bony landmarks or vascular bifurcations, rather than external fiducial markers.

CONCLUSIONS

In this early clinical experience, MRI-derived road-maps added information to a range of invasive cardiovascular procedures including graft coronary arteriography, cardiac tumor biopsy, and peripheral artery intervention. In some cases, MRI-derived roadmaps outperformed best-available imaging modalities. In others, external fiducial markers shifted with underlying loose skin, especially over the abdomen, causing registration error. X-ray fusion with MRI roadmaps is feasible and may prove a valuable adjunct to invasive cardiovascular procedures. With further development, XFM or related adjunctive imaging may improve the safety and success rate of a range of complex endovascular interventions, and may bring complex interventional procedures to a broader base of physicians by making them simpler to perform.

Supplementary Material

Refer to Web version on PubMed Central for supplementary material.

Acknowledgements

References

1. Turski PA, Stieghorst MF, Strother CM, Crummy AB, Lieberman RP, Mistretta CA. Digital subtraction angiography "road map". AJR Am J Roentgenol 1982;139:1233–1234. [PubMed: 6983278]

2. Sra J, Krum D, Malloy A, Vass M, Belanger B, Soubelet E, Vaillant R, Akhtar M. Registration of three-dimensional left atrial computed tomographic images with projection images obtained using fluoroscopy. Circulation 2005;112:3763–3768. [PubMed: 16344405]

3. Dong J, Calkins H, Solomon SB, Lai S, Dalal D, et al. Integrated electroanatomic mapping with three-dimensional computed tomographic images for real-time guided ablations. Circulation 2006;113:186–194. [PubMed: 16401772]

4. Dickfeld T, Calkins H, Zviman M, Kato R, Meininger G, Lickfett L, Berger R, Halperin H, Solomon SB. Anatomic stereotactic catheter ablation on three-dimensional magnetic resonance images in real time. Circulation 2003;108:2407–2413. [PubMed: 14568905]

5. Ector J, De Buck S, Adams J, Dymarkowski S, Bogaert J, Maes F, Heidbuchel H. Cardiac three-dimensional magnetic resonance imaging and fluoroscopy merging: A new approach for electroanatomic mapping to assist catheter ablation. Circulation 2005;112:3769–3776. [PubMed: 16330683]

6. Wacker FK, Vogt S, Khamene A, Jesberger JA, Nour SG, Elgort DR, Sauer F, Duerk JL, Lewin JS. An augmented reality system for MR image-guided needle biopsy: initial results in a swine model. Radiology 2006;238:497–504. [PubMed: 16436814]

7. Rhode KS, Sermesant M, Brogan D, Hegde S, Hipwell J, et al. A system for real-time XMR guided cardiovascular intervention. IEEE Trans Med Imaging 2005;24:1428–1440. [PubMed: 16279080]

8. Fitzpatrick JM, West JB, Maurer CR Jr. Predicting error in rigid-body point-based registration. IEEE Trans Med Imaging 1998;17:694–702. [PubMed: 9874293]

9. Tomazevic D, Likar B, Slivnik T, Pernus F. 3-D/2-D registration of CT and MR to X-ray images. IEEE Trans Med Imaging 2003;22:1407–1416. [PubMed: 14606674]

10. Penney GP, Weese J, Little JA, Desmedt P, Hill DL, Hawkes DJ. A comparison of similarity measures for use in 2-D-3-D medical image registration. IEEE Trans Med Imaging 1998;17:586–595. [PubMed: 9845314]

11. Gutierrez LF, Schechter G, Lederman RJ, McVeigh ER, Ozturk C. Distortion correction, calibration and registration: Toward and integrated MR and X-ray interventional suite. Proc SPIE 2005;5744:146–156.

12. de Silva R, Gutierrez LF, Raval AN, McVeigh ER, Ozturk C, Lederman RJ. X-ray fused with magnetic resonance imaging (XFM) to target endomyocardial injections: Validation in a swine model of myocardial infarction. Circulation 2006;114:2342–2350. [PubMed: 17101858]

13. Sampath S, Raval AN, Lederman RJ, McVeigh ER. High-resolution 3D arteriography of chronic total peripheral occlusions using a T1-W turbo spin-echo sequence with inner-volume imaging. Magn Reson Med 2007;57:40–49. [PubMed: 17152076]

14. Jovicich J, Czanner S, Greve D, Haley E, van der Kouwe A, et al. Reliability in multi-site structural MRI studies: Effects of gradient non-linearity correction on phantom and human data. Neuroimage 2006;30:436–443. [PubMed: 16300968]

15. McLeish K, Hill DL, Atkinson D, Blackall JM, Razavi R. A study of the motion and deformation of the heart due to respiration. IEEE Trans Med Imaging 2002;21:1142–1150. [PubMed: 12564882]

16. Noseworthy PA, Malchano ZJ, Ahmed J, Holmvang G, Ruskin JN, Reddy VY. The impact of respiration on left atrial and pulmonary venous anatomy: Implications for image-guided intervention. Heart Rhythm 2005;2:1173–1178. [PubMed: 16253905]

17. Shechter G, Resar JR, McVeigh ER. Displacement and velocity of the coronary arteries: Cardiac and respiratory motion. IEEE Trans Med Imaging 2006;25:369–375. [PubMed: 16524092]

18. von Siebenthal M, Szekely G, Gamper U, Boesiger P, Lomax A, Cattin P. 4D MR imaging of respiratory organ motion and its variability. Phys Med Biol 2007;52:1547–1564. [PubMed: 17327648]

19. Tobis J, Johnston WD, Montelli S, Henderson E, Roeck W, Bauer B, Nalcioglu O, Henry W. Digital coronary roadmapping as an aid for performing coronary angioplasty. Am J Cardiol 1985;56:237–241. [PubMed: 3161319]

20. Garcia JA, Chen J, Hansgen A, Wink O, Movassaghi B, Messenger JC. Rotational angiography (RA) and three-dimensional imaging (3-DRA): An available clinical tool. Int J Cardiovasc Imaging 2007;23:9–13. [PubMed: 16779617]

21. Hawkes DJ, Barratt D, Blackall JM, Chan C, Edwards PJ, Rhode K, Penney GP, McClelland J, Hill DL. Tissue deformation and shape models in image-guided interventions: a discussion paper. Med Image Anal 2005;9:163–175. [PubMed: 15721231]

22. Orford JL, Lerman A, Holmes DR. Routine intravascular ultrasound guidance of percutaneous coronary intervention: A critical reappraisal. J Am Coll Cardiac 2004;43:1335–1342.
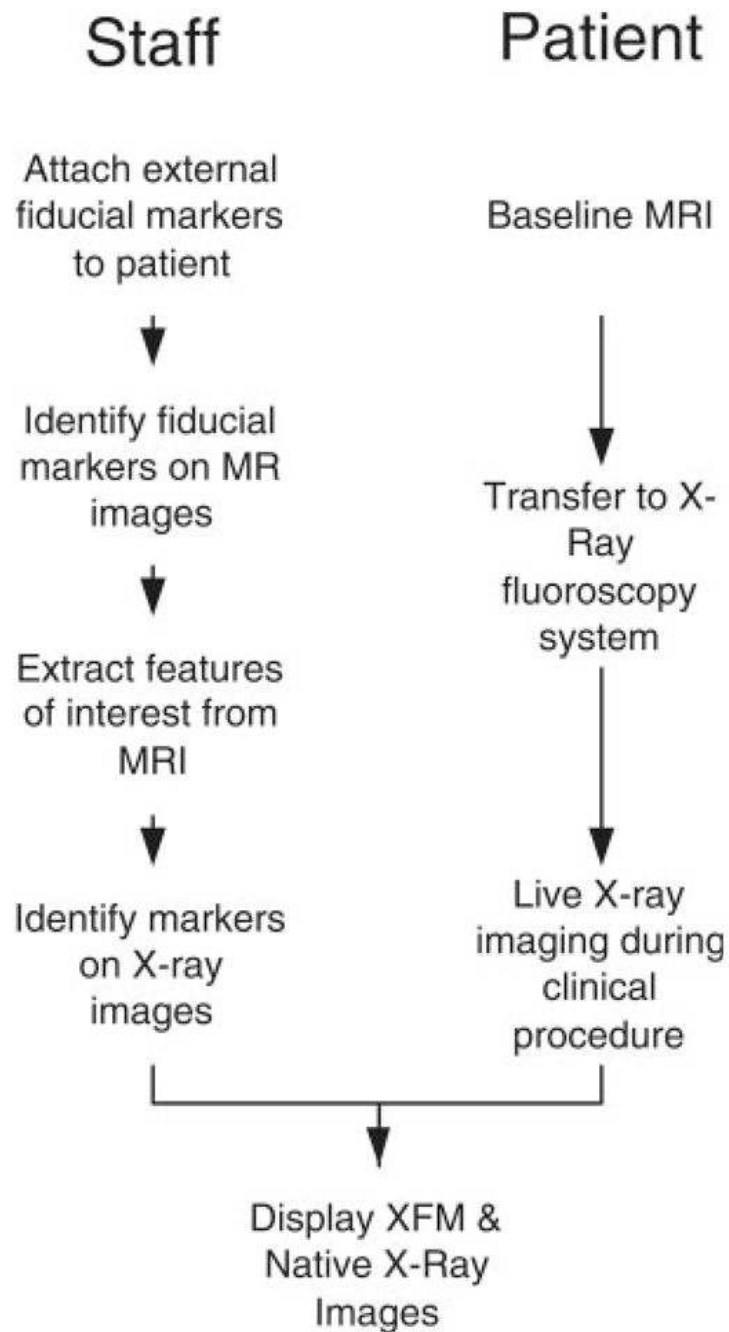
Staff

Patient

Attach external
fiducial markers
to patient

Baseline MRI

↓

Identify fiducial
markers on MR
images

↓

Transfer to X-
Ray
fluoroscopy
system

Extract features
of interest from
MRI

↓

↓

Identify markers
on X-ray
images

Live X-ray
imaging during
clinical
procedure

↓

Display XFM &
Native X-Ray
Images

Fig. 1.
Staff and patient workflow during XFM procedures. Baseline MRI is performed after fiducial markers are affixed to patients' skin. Although the patient is transferred to the X-ray system, the fiducial markers and MRI regions of interest are manually extracted. The fiducial markers are identified on X-ray and image fields are registered. Afterward, the 3D and 2D images are transformed and combined during live X-ray imaging.
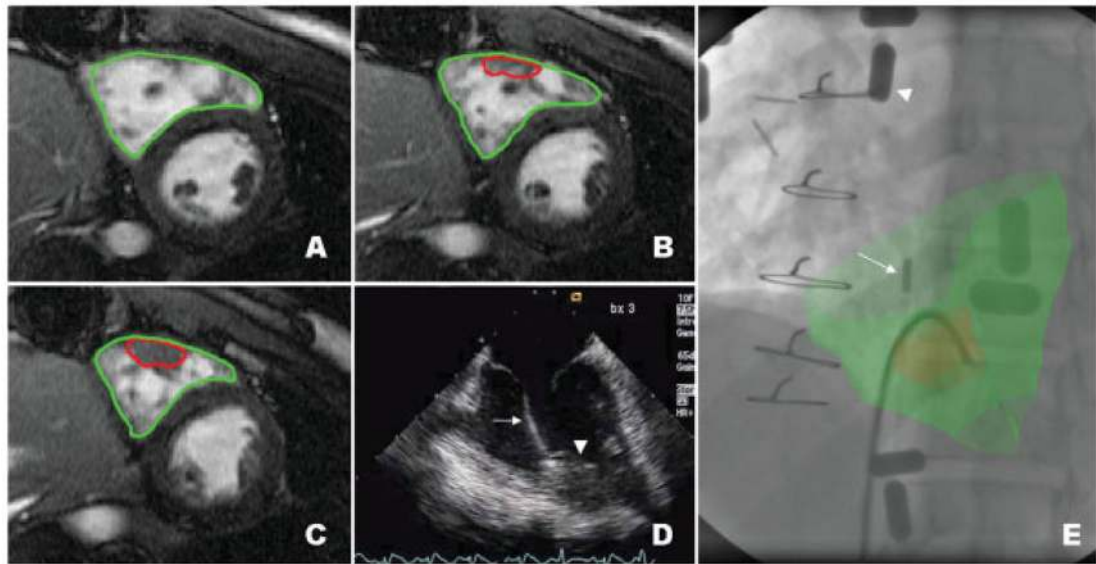
Fig. 2.
XFM-guided biopsy of a mass in the right ventricular free wall. Serial thin section SSFP MR images (panels A–C) with manually segmented regions of interest depicting the right ventricular endocardial border (green) and the mass in free wall (red). Panel D shows an intracardiac echocardiogram of the bioptome (arrow) engaging the mass (arrowhead). Panel E shows the XFM image. External fiducial markers are affixed to the skin (example marked with arrowhead). The intracardiac ultrasound catheter is positioned in the right atrium (arrow). The MRI-derived regions of interest (red and green) are overlaid on live X-ray and corroborate positioning of the bioptome.
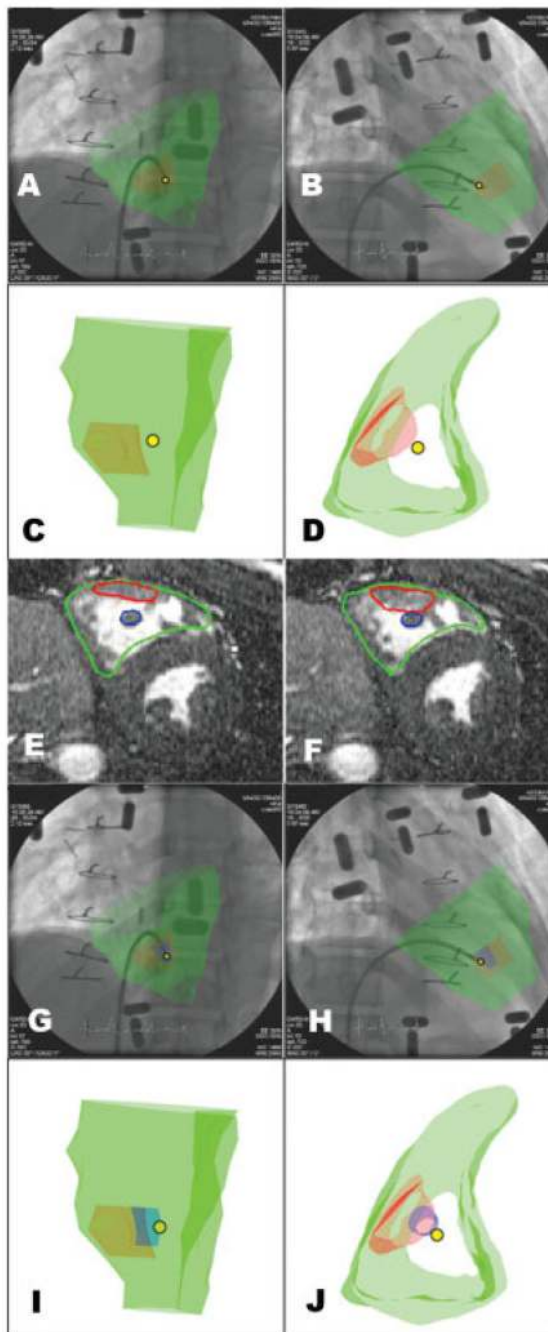
Fig. 3.
Triangulating the position of the bioptome. Panels A–B show two different fluoroscopic projections and corresponding 3D MRI-derived regions of interest (C, D). The right ventricular endocardial border is depicted in green, the mass in red, and the tip of the biopsy forceps is depicted as a yellow dot. The bioptome is discontiguous with the mass (see text). Panels E–J provide an explanation for the spurious normal biopsy finding. Review of MRI (panels E and F) reveals a papillary muscle (blue) posterior to the mass (red). Revised XFM (G–H) incorporates the papillary muscle. Panels I–J shows the 3D image of the mass (red), papillary muscle (blue), and triangulated bioptome position (yellow dot) indicating that the specimens were obtained from the papillary muscle and not from the mass.

Fig. 4.
XFM using a 3D contrast-enhanced MR angiogram. (A) shows a retrograde L iliac radiocontrast angiogram in a contralateral oblique projection. (B) shows the regions of interest (adventitial borders, green) derived from a T1-weighted noncontrast MRI. (C) shows the XFM of both X-ray and MR angiograms. The correspondence is high.
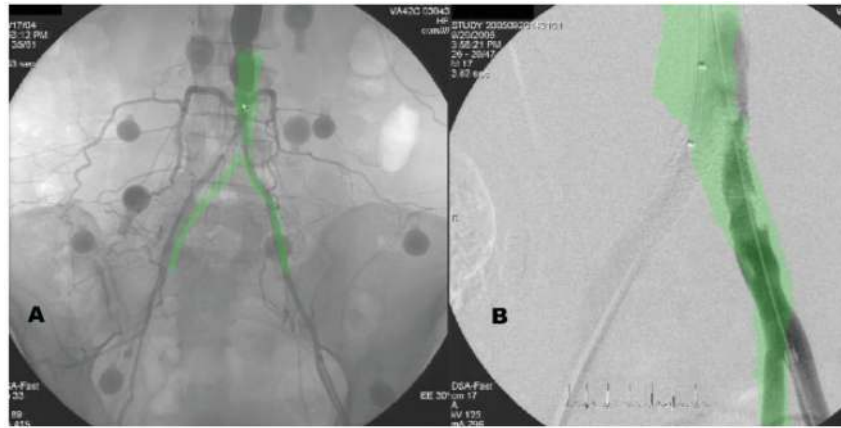
Fig. 5.
Unsatisfactory registration during an iliac artery revascularization procedure. Panel A shows the misregistration of a contrast-enhanced MR angiogram with X-ray during XFM. Multiple fiducial markers are positioned on the abdominal skin. Panel B shows another patient with MR-derived arterial adventitial contours overlaid during recanalization of occlusive iliac in-stent restenosis. Both presumably reflect error introduced by nonrigid deformation and respiratory motion of the fiducial markers.
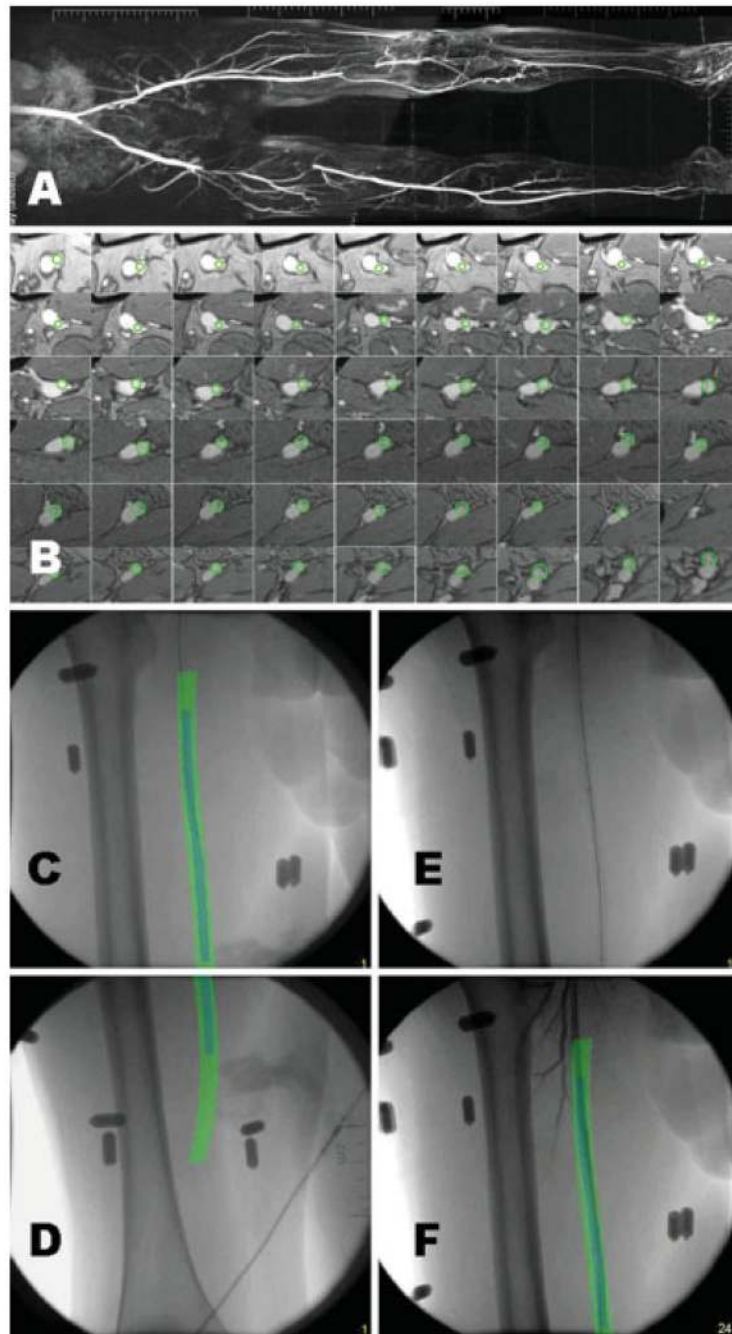
Fig. 6.
XFM-guided recanalization and stenting of R superficial femoral artery occlusion. A: Baseline composite contrast-enhanced MR angiogram shows R SFA occlusion and contra-lateral popliteal and tibial occlusion. B: A descending series of axial T1-weighted MR images permit contrast-independent arterial contours to be segmented (green). C and D: The MRI-derived contours are combined in XFM with the live X-ray images during guidewire recanalization. Note that the automatic gantry position correction permits the same XFM contours to be applied throughout the occlusion, which spans two X-ray fields of view. E: X-ray image after stenting. F: XFM during final poststent angiography.
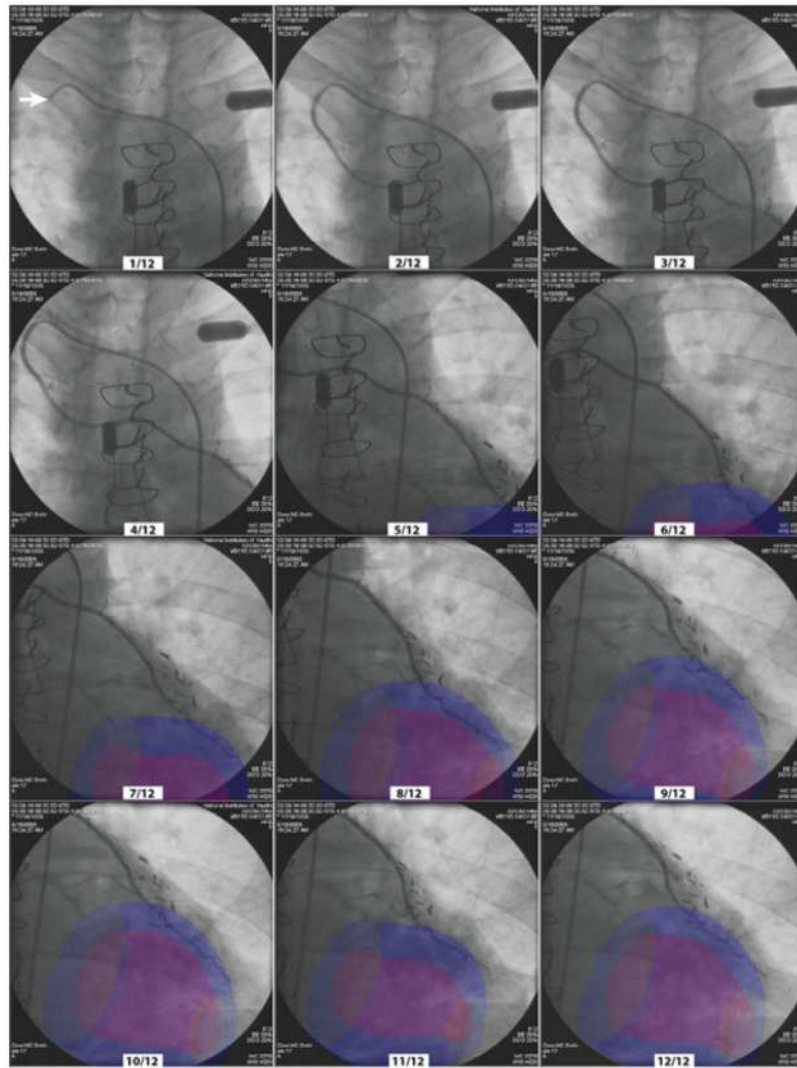
Fig. 7.
XFM during graft coronary arteriography. An injection sequence of a right internal mammary artery during ECG-gated XFM with continuous table panning. The corresponding numbered phase of the cardiac cycle is correctly represented by the MRI-derived regions of interest, irrespective of table position, throughout the injection. [Color figure can be viewed in the online issue, which is available at www.interscience.wiley.com.]